Design Optimization for UAV Aided Sustainable 3D Wireless Communication at mmWaves

Nancy Varshney and Swades De

***Abstract*—Unmanned aerial vehicles (UAVs) operating at different altitudes will be integral to the 5th generation and beyond (5G+) communication network to provide ubiquitous coverage. Though 5G+ communications target to operate in sub-6 GHz as well as millimeter wave range (mmWaves), sub-6 GHz being already congested, mmWaves are seen as a viable technology that can support high data rates. To this end, in this paper, we study the feasibility of using UAVs at mmWaves deployed at low altitudes to serve a user population higher than the number of RF chains available at the UAV. Since the UAVs are energy constrained devices, solar harvesting is considered for the UAVs to act as access nodes for an extended period of time. Practical 3-dimensional antenna array radiation pattern and the resulting inter-beam interference from the sidelobes are taken into account in the analysis. We devise a sub-array hybrid precoder that provides minimum rate support to all users across the wideband mmWave channel. The RF precoder is designed according to the users' locations. In addition, we propose a low complexity iterative joint subcarrier allocation and baseband precoder optimization algorithm with faster convergence. In the proposed algorithm, we employ weighted minimum mean squared error (WMMSE) to design baseband precoder to reduce inter-beam interference while jointly optimizing subcarrier allocation to maintain minimum user rate constraint. Next, we determine the optimal number of beams at UAV to optimize throughput while guaranteeing minimum user rate support for energy sustainable UAV operation. Finally, we compare the performance gain achieved by low-altitude UAV deployed at mmWaves over the UAV deployed at sub-6 GHz frequency range.**

***Index Terms*—Energy sustainable system, hybrid beamforming, minimum rate, solar powered communication, unmanned aerial vehicle (UAV).**

I. Introduction

The 5th generation and beyond (5G+) communication envisions to provide three-dimensional (3D) ubiquitous coverage. Unmanned aerial vehicle (UAV)-assisted communication integrated with terrestrial communication will play a vital role in delivering unprecedented coverage. Inherent ease of deployment and freedom of movement will allow UAVs to act as aerial base stations and aerial relays. Guidelines for UAV deployment as users at sub-6 GHz frequency range are already specified in release 17 of the third-generation partnership project (3GPP) [1]. For 5G+ communications, sub-6 GHz, millimeter waves (mmWaves), and terahertz frequency bands are proposed. Among these, sub-6 GHz and mmWave frequency bands are more suitable for low-altitude UAVs. High attenuation, atmospheric absorption, and very narrow beams at terahertz range lead to a very small coverage area. Thus, using terahertz frequency for low-altitude UAVs is not justified.

Research on low-altitude UAVs at the sub-6 GHz range has shown that UAVs can be used to overcome blockages in dense blockage environments [2]. These can further be used for extending the coverage in hotspots, temporary coverage in rural areas, and in disaster recovery with reduced capital expenditure. Benefited by freedom of movement and higher altitude, the UAVs can establish line-of-sight (LoS) links. This is especially helpful at mmWaves, where terrestrial communication often suffers from non-line-of-sight (NLoS) links [3]. The study in [4] suggested that it is beneficial to use mmWaves at UAV when high data rates are required, whereas sub-6 GHz operation is suitable when lower data rates with broader coverage is needed. Therefore, deploying UAVs at mmWaves is beneficial in providing more bandwidth and strong LoS links resulting in high data rates that can be enhanced further by beamforming and spatial multiplexing. However, its increased power requirements, reduced range, and computational complexity pose challenges at mmWaves.

Power consumption by the UAV is another critical factor in UAV-assisted communications because of the energy constraints at the UAV. The rotary-wing UAVs can perform static hovering and hence overcome the problem of beam misalignment to a large extent, which makes them perfect for use as low-altitude aerial base stations at mmWaves [5]. However, these UAVs consume a lot of power because of their unique structural design, requiring more propulsion energy. The current battery technology allows for a maximum of 1 to 2 hours of UAV operation. This duration can be extended by powering the UAV with renewable energies. Solar energy is one such readily available energy at UAV. For instance, Facebook Aquila project aims to provide network coverage by solar-powered high-altitude UAVs. In this, to cover an area of 100 km^2, the high-altitude UAV needs wing length of at least 36 m to harvest the required solar power for sustaining the UAV operation [6]. Therefore, with the vision of UAV integration in 5G+ communications, it is now crucial to investigate sustainable UAV operation at mmWave range.

II. Background and Contributions

A. Related works

The majority of research work on UAV-assisted communication have been undertaken in the sub-6 GHz frequencies, covering optimal 3D placement, path planning, channel modeling,

N. Varshney and S. De are with the Department of Electrical Engineering and Bharti School of Telecommunication, Indian Institute of Technology Delhi, New Delhi, India (e-mail: bsz188118@iitd.ac.in, swadesd@ee.iitd.ac.in).

backhaul connectivity, security and privacy challenges, energy limitations, and many other [7], [8]. However, the sub-6 GHz study cannot be applied to mmWaves since its channel model and antenna designs are different [9]. The investigation of the feasibility of UAV operation at mmWaves is still in its infancy. The study in [10], [11] conducted ray-tracing simulations using the Wireless Insite tool by Remcom to study the urban air-to-ground channel for UAVs deployed at low altitudes of 80-120 meters at 28 GHz and observed that coverage improves upto certain altitudes because of better LoS connectivity that in turn improves the achievable SNR. For different UAV heights and blockage scenarios, the authors in [12] investigated the mmWaves outage probability. The work in [13] studied UAV as an aerial relay node to provide flexible aerial backhaul links when the terrestrial links suffer blockages. However, little consideration has been given to UAVs acting as base stations to serve multiple users at mmWave frequency.

The work in [14] studied the optimal placement and orientation of mmWave enabled UAV as a base station so that the users have guaranteed LoS coverage. In [15], mmWaves enabled UAV is deployed to serve multiple users over narrowband channels, but this work considered that each user gets a dedicated data stream generated from a single RF chain, thereby limiting the maximum number of users supported at a time instant. Further, due to power constraints and limited number of RF chains, sub-array hybrid precoding architecture is suited for UAVs acting as base stations. Such a hybrid precoder comprises an analog (or RF) precoder and a digital (or baseband) precoder. In hybrid precoder, steering of the beam induces interference to users located in other beams. To overcome inter-beam interference the authors in [16] maximized the rate of each user by steering the beam towards its dominant multipath component (MPC) while maintaining the minimum rate constraint of the rest of the users. This approach is feasible when the number of users is not more than the number of RF chains. In a multi-user scenario, with the number of users greater than the number of RF chains available at the UAV, the work in [17] grouped the users using cell sectoring method and served multiple users in a group via orthogonal frequency division multiple access (OFDMA). For this system, the authors studied the sum rate variation as a function of deployment height, number of antennas, and backhaul link capacity. Though the authors considered the inter-beam interference, they used an approximated antenna array gain pattern. Moreover, they did not use any baseband precoder to mitigate the interference; instead considered only subcarrier assignment optimization for the users in presence of interference. In [18], beam space precoding via discrete lens arrays was analyzed to reduce UAV hardware cost to support a multi-user communication at mmWaves.

Additionally, energy efficiency is an important factor to consider for long-term UAV-assisted communications. The works in [19], [20] studied different energy efficient schemes for communication with rotary-wing UAVs. To improve the energy efficiency of UAV-assisted communication systems at mmWaves, a set of studies targeted optimizing the resource allocation, coverage or trajectory optimization [21]–[23]. Recently, sustainable solar-powered UAVs communication designs are being investigated in the literature. The authors in [24] proposed optimal resource allocation design and 3D trajectory route design for an energy-constrained solar-powered UAV. The studies in [25], [26] also presented energy efficient algorithms for a solar-powered UAV. However, the limitations of these studies are that they focused on the sub-6 GHz band and attempted to enhance energy efficiency using solar power harvested in real time. These studies did not look at the solar panel size optimization for providing an energy efficient system for serving users on a long-term basis.

B. Motivation and contribution

In this paper we consider solar-powered UAV deployed at fixed height that act as aerial base station to provide ad hoc connectivity at mmWaves with minimum QoS guarantee to a non-homogeneously distributed terrestrial user population. The user population considered is much larger than the number of RF chains available at the UAV. We investigate the system performance by considering practical antenna radiation pattern and the resulting sidelobe interference, wherein we exploit the fact that at mmWaves, large number of antenna elements can be placed on the UAV to provide narrow steerable beams to serve the terrestrial population.

The prior works combinedly designed the RF precoder and the baseband precoders using zero-forcing (ZF) precoder or minimum mean square error (MMSE) precoders to minimize inter-user interference with a prior subcarrier allocation in a multi-user scenario. The limitation of ZF and MMSE precoders is that the objective of these precoders is to achieve maximum sum rate, and hence do not guarantee minimum QoS to all the users in the system. To meet the QoS requirement while using ZF precoding, the work in [15] optimized the power over different data streams for fully-connected hybrid architecture. Besides the complexity of joint RF precoder, baseband precoder, and greedy user grouping algorithm in [15], the convergence rate of the proposed power allocation algorithm to satisfy QoS of all the users is very slow. In our prior work [27], we have shown that at mmWaves it is beneficial to first group users and then perform subcarrier allocation and baseband precoding leveraging beam squint. Moreover, with an aerial base station capable of generating narrow steerable beams, it is beneficial to group the users based on their positions rather than dividing the area into sectors as in [17].

From an energy efficiency standpoint, the closest work that considers the effect of the UAV power limits on the aerial communication system performance is presented in [26]. However, it considered the sub-6 GHz operation with a single RF chain generating a fixed beam of null-to-null beamwidth of 120^o. At mmWaves, the hardware power consumption caused by a large number of RF chains is significant. Therefore, in this work we estimate the optimal number of narrow beams for energy efficient UAV operation for a given power budget. Further, we find that, in addition to the power consumed by transmission and RF hardware units, the power consumed in UAV hovering has an effect on system energy efficiency and hardware design parameters, such as solar panel sizing.

When using a solar-powered UAV, the solar panel should support UAV hovering as well as communication and battery charging. The solar panel, on the other hand, adds weight, which increases hovering power and thus affects the UAV performance. To this end, solar panel design optimization is investigated in this study for a comprehensive analysis of sustainable UAV operation. The novel contributions and scope of our work are summarized below.

a) A multi-user UAV-assisted communication system at mmWaves with minimum QoS requirements is presented for users distributed non-homogeneously over a small region. At UAV, user grouping is carried out and the users in one group are served by a single RF chain employing OFDMA.
b) User grouping using k-means clustering is proposed with adjustable beamwidth in azimuth and elevation plane. Using Monte Carlo simulation results, it is demonstrated that user grouping using the k-means clustering approach outperforms user grouping using the sectoring approach.
c) Subsequently, a low-complexity joint subcarrier allocation and baseband precoder optimization is devised that assures QoS to all users at a faster convergence rate. It consists of an iterative algorithmic solution in which the subcarrier allocation and baseband precoder are adjusted iteratively to preserve the required QoS while minimizing inter-beam interference.
d) Additionally, the estimation of the optimal number of beams for long-term UAV-assisted communications is presented. The effect of solar panel size on the energy efficiency of UAV-assisted mmWaves communication is also investigated.
e) Finally, the performance of the UAV-assisted communication system at mmWaves is compared to that operating at sub-6 GHz, highlighting the limitation of backhaul power on fronthaul communication at sub-6 GHz versus that at mmWaves.

It is notable that, optimum UAV hovering system design for solar powered communication to the ground users at mmWaves, considered in the study, is the first basic design optimization. Accordingly, the aspects of UAV mobility and multi-UAV cooperation at mmWaves are not in the scope of current study.

C. Organization

The system model is presented in Section III. User grouping and RF precoder design optimization problems are presented in Section IV. Subcarrier and baseband precoder optimization with QoS constraint are presented in Section V. UAV battery design and solar panel design are discussed in Section VI. The simulation results are presented in Section VII, and the concluding remarks are drawn in Section VIII.

Notations: For a vector A, $A(n)$ indicates the nth element of the vector. $|\cdot|$ denotes cardinality and $\mathcal{O}$ denotes algorithm run-time complexity. $[x]^+$ is equivalent to $\max(x, 0)$.

III. System Model

The UAV communication system model and the UAV power consumption model at mmWaves are presented in this section.

A. mmWave UAV communication system model

We consider a multi-user urban microcellular (UMi) scenario, where a UAV serves a total of K users. The UAV has a backhaul connectivity with a gNodeB (gNB) situated at a 2-dimensional (2D) distance of $d_{UAV-gNB}$ m. The height of gNB is h_{gNB}. The users are single antenna devices with antenna gain G_r. The users on the ground are distributed in a circular area $\mathcal{A} \in \mathbb{R}^2$ with a radius $\mathcal{R}$ following the Cox point process. When a UAV hovers in one location, it uses the least amount of energy. Hence, we assume the UAV hovers at a fixed position throughout the transmission duration for an energy-efficient mmWaves system. Besides, in order to boost fronthaul rates, UAV-to-user path loss should be minimized. Therefore, UAVs are deployed close to users, i.e., above the center of $\mathcal{A}$ at h_U height, to lower the average UAV-to-user distance during the entire communication period.

The UAV consists of N_B RF units for fronthaul communication and one RF unit for backhaul connection. Also, on the UAV we consider two set of uniform planar arrays (UPA), one for fronthaul transmission and one for backhaul transmission. One UPA of dimensions $\sqrt{N_t} \times \sqrt{N_t}$ is connected to N_B RF units in fronthaul to serve the users and the other UPA with dimensions $\sqrt{N_b} \times \sqrt{N_b}$ is connected to backhaul unit to generate pointed backhaul link to the gNB. At gNB, $\sqrt{N_g} \times \sqrt{N_g}$ array panel is used for establishing backhaul link to the UAV. The response vector of an UPA at an azimuth angle ϕ and elevation angle θ is given as

$$\mathbf{a}_T(f,\phi,\theta) = \frac{1}{\sqrt{N_t}}\Big[1,\ldots,e^{\frac{-j2\pi d'}{\lambda_c}\frac{f}{f_c}\sin\theta[(m-1)\cos\phi+(n-1)\sin\phi]} \\ ,\ldots,e^{\frac{-j2\pi}{\lambda_c}\frac{f}{f_c}d'\sin\theta\left[(\sqrt{N_t}-1)\cos\phi+(\sqrt{N_t}-1)\sin\phi\right]}\Big]^T \in \mathbb{C}^{1\times N_t} \tag{1}$$

where f/f_c is the beam squint factor at frequency f, d' is the inter element ULA spacing, λ_c is the carrier wavelength, and m and n indices represent the m^{th} and n^{th} antenna element, respectively, along the x-axis and y-axis of the UPA.

Due to shadowing from buildings, the air-to-ground links between the user and the UAV are either line-of-sight (LoS) or non-line-of-sight (NLoS) links. In this work, we follow the 3GPP UMi street canyon LoS probability model given as [28]

$$\mathbb{P} = \prod_{a=0}^{b}\left[1-\exp\left(\frac{-h_U-\frac{(a+0.5)h_U}{b+1}}{2\omega^2}\right)\right] \tag{2}$$

where $b = \lfloor d_k\sqrt{\xi\varsigma} - 1\rfloor$, d_k is the 2D distance between the UAV and the user k, and description of ς, ξ, and ω are given in Table I. Additionally, the path loss for LoS and NLoS link for the k^{th} user, at a 2D distance d_k from the UAV are obtained as [10]

$$PL_{los}(d_k) = a_L + n_L 10\log_{10}(\sqrt{d_k^2+h_U^2}) + \mathcal{N}(0,\sigma_L^2) \text{ [dB]} \\ PL_{nlos}(d_k) = a_N + n_N 10\log_{10}(\sqrt{d_k^2+h_U^2}) + \mathcal{N}(0,\sigma_N^2) \text{ [dB]}. \tag{3}$$

Here, a_L and a_N are frequency dependent constants, n_L and n_N are path loss exponents, and σ_L^2 and σ_N^2 are shadowing

Table I: Some important variable description

Acronym	Description
$\mathbf{a_T}$	UPA response vector
B	Bandwidth
d_k	2D distance of user k from the UAV
$d_{UAV-gNB}$	UAV to gNB 2D distance
f_c	Carrier frequency
f_n	Carrier frequency of n^{th} subcarrier
G_r	Single antenna element gain of user
G_0	Single antenna element gain of UPA
h_U	UAV height in meters
h_{gNB}	gNB height in meters
$\mathbf{h}_k$	User to UAV channel of user k
K	User population
L_k	Total number of MPCs of k^{th} user
N_0	Noise one-sided power spectral density
N_c	Number of subcarriers
N_B	Number of RF chains/beams at UAV
N_b	Total number of antenna elements at UAV for backhaul
N_g	Total number of antenna elements at gNB for backhaul
N_t	Total number of antenna elements at UAV for fronthaul
PL_k	Linear path loss of user k
R_0	Minimum user rate (or QoS rate) requirements
$\alpha_{k,l}$	Small scale fading gain of l^{th} MPC of k^{th} user
$\phi_{k,l}$	Azimuth AoA of l^{th} MPC of k^{th} user
$\theta_{k,l}$	Elevation AoA of l^{th} MPC of k^{th} user
Φ_j	Azimuth HPBW of j^{th} beam
Θ_j	Elevation HPBW of j^{th} beam
$\bar{\phi}_j$	Azimuth steering angle of j^{th} beam
$\bar{\theta}_j$	Elevation steering angle of j^{th} beam
$\mathbb{P}$	LoS probability of a link
κ	Ricean parameter
ξ	Ratio of area occupied by buildings to total area
ς	Mean number of building per unit area
ω	Building height distribution parameter
α'	Number of rotors in rotary winged UAV
β	Area of a spinning blade of UAV
ρ	Air density

variances respectively for LoS and NLoS links. Therefore, the linear path loss for k^{th} user is

$$\text{PL}_k = 10^{[\mathbb{P}PL_{los}(d_k)+(1-\mathbb{P})PL_{nlos}(d_k)]/10}. \tag{4}$$

The mmWave wideband channel exhibits frequency selective fading. Therefore, the total bandwidth B is divided into N_c narrowband channels. Further, the channel consists of $L_k \ll N_t$ multipath components (MPCs). Thus, the channel between the UAV and the k^{th} user over the n^{th} subcarrier at frequency f_n is expressed as

$$\mathbf{h}_k[n] = \sqrt{\frac{N_t}{L_k \text{PL}_k}} \sum_{l=1}^{L_k} \alpha_{k,n,l} \mathbf{a_T}(f_n, \phi_{k,l}, \theta_{k,l})^H \in \mathbb{C}^{1\times N_t} \tag{5}$$

where $\alpha_{k,n,l}$ is complex fading gain of l^{th} multi-path component (MPC) over subcarrier n and $\phi_{k,l}$ and $\theta_{k,l}$ are angle-of-arrival (AoA) of l^{th} MPC in azimuth and elevation plane, respectively, assumed to be uniformly distributed with angular spread of σ_T^{AS}. We assume that UAV has perfect knowledge of all users' channel state information (CSI) and positions.

B. Power consumption model

UAV power consumption comprises three main components: in transmission, in communication circuit board, and in UAV motion.

Table II: Power consumption of components in a RF chain.

Component	Notation	Power consumption
RF transceiver	P_{RF}	293 mW per RF chain [29]
Phase-shifter	P_{PS}	0 mW per antenna [30]
Power amplifiers	P_{PA}	P_T/η_{PA}
Power amplifier efficiency	η_{PA}	47% [31]

1) Power consumed in transmission: The transmission power in UAV is the total power required for data transmission, composed of the power consumed in fronthaul transmission P_T and the power consumed in backhaul communication P_B.

2) Power consumption in RF module: The RF transmitting module power consists of the power consumed in RF front end components like analog-to-digital converter/digital-to-analog converter (ADC/DAC), RF mixer, and local oscillator. We denote the collection of all these components as an RF transceiver having power consumption P_{RF}. Phase shifters connected to antenna elements are passive, and hence they have zero power consumption. In addition, the power amplifiers (PAs) in RF circuit boards are energy-hungry devices with efficiency η_{PA}. The power consumption values and quantities of all the components in an RF front end are listed in Table II [29]. Therefore, the total power consumption in a communication module is given as

$$P_C = \underbrace{P_T + P_B}_{\text{Transmission power}} + \underbrace{(N_B+1)P_{RF} + \eta_{PA}(P_T+P_B)}_{\text{Power consumed in mmWave transmission module}}. \tag{6}$$

Here the term $(N_B + 1)$ represents the total number of RF chains at the UAV (N_B for fronthaul and 1 for backhaul).

3) Power consumption in UAV motion: In this work we assume static UAV position hovering at height h_U. Air speed is zero during hovering and thrust balances the UAV weight force. Therefore, the total thrust is

$$T = g(m_1 + m_2 + m_3 + m_4) \tag{7}$$

where m_1, m_2, m_3 and m_4, respectively, represent the masses of UAV body, battery, and solar panel, and payload, and g is the gravity. Therefore, the hovering power required for the rotary-wing UAV is [32]

$$P_{hover} = \frac{T^{3/2}}{\sqrt{2\alpha\rho\beta}} = \frac{g(\sum_{i=1}^{4} m_i)^{3/2}}{\sqrt{2\alpha'\rho\beta}} \tag{8}$$

where α is the number of of rotors, ρ is air density, β is the area of spinning blade.

IV. User Grouping and RF Precoder Design

We consider a two-stage hybrid precoder design. First, the RF precoder is designed based on users' geometric information, and then the rate performance of the system is optimized at the baseband level. This section focuses on the RF precoder design by grouping users. For this, we consider a sub-array hybrid precoder architecture in which each RF unit is connected to a set of non-overlapping antenna elements that generates a single steerable beam. Users in each group are served over the wideband mmWave channel by employing OFDMA. Let $\mathcal{K}_j$ denote the set of users in group j, where $j = \{1, \ldots, N_B\}$.

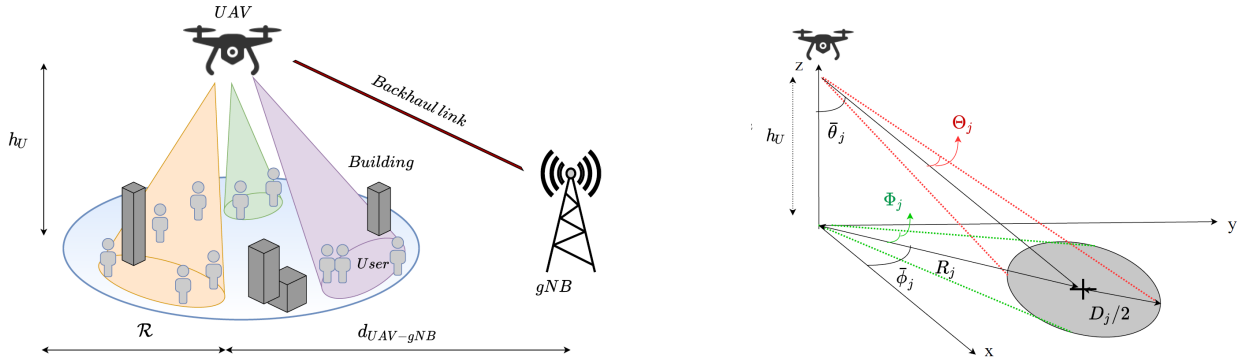

(a) (b)

Figure 1: (a) Illustration of user grouping to partition users into $N_B^{k\text{-means}} = 3$ groups using k-means clustering. (b) Geometric illustration of steering angles and beamwidth in azimuth and elevation planes.

The UAV divides the users into $N_B = N_B^{k\text{-means}}$ groups using k-means clustering, and each group is served by one RF beam, (Fig. 1(a)). By activating the needed number of antenna elements in the UPA, the beamwidth can be adjusted to optimize the coverage that is sufficient enough to cover the users in the group. Let $x_m \in \mathbb{R}^2$ denote the Cartesian coordinates of the m^{th} user. Then the maximum diameter $\mathcal{D}_j$ of the spot covering the $\mathcal{K}_j$ users of j^{th} group is

$$\mathcal{D}_j = \max_{m,n \in \mathcal{K}_j} (||x_m - x_n||_2). \tag{9}$$

Thus, the UAV refines each beam's azimuth and elevation beamwidth depending on the user positions within in the group to focus maximum beam radiation towards the users (Fig. 1(b)). The half-power azimuth beamwidth Φ_j and elevation beamwidth Θ_j for j^{th} beam are the set as

$$\begin{aligned} \Phi_j &= \tan^{-1} \frac{\mathcal{D}_j/2}{\mathcal{R}_j} \\ \Theta_j &= \tan^{-1}\left(\frac{\mathcal{R}_j}{h_U}\right) - \tan^{-1}\left(\frac{\mathcal{R}_j - \mathcal{D}_j/2}{h_U}\right) \end{aligned} \tag{10}$$

where $\mathcal{R}_j$ is the 2D distance of j^{th} group center from the UAV.

$\sqrt{N_T} \times \sqrt{N_T}$ UPA is partitioned into $N_B^{k\text{-means}}$ subarrays of dimensions $\sqrt{N_j} \times \sqrt{N_j}$ such that $\sum_{j=1}^{N_{RF}} \sqrt{N_j} \times \sum_{j=1}^{N_{RF}} \sqrt{N_j} = \sqrt{N_T} \times \sqrt{N_T}$. The value of N_j is determined as follows [33]

$$N_j = \min\left(\left\lceil \frac{2.782}{\pi \sin(\max\{\Phi_j, \Theta_j\}) \cos(\tan^{-1}\frac{d_k}{h_U})} \right\rceil, N_{max}\right) \tag{11}$$

where N_{max} is the upper bound on the active number of antenna elements in a sub-array. The steering direction of j^{th} beam in azimuth and elevation plane, respectively, are

$$\tilde{\phi}_j = \mathop{\mathbb{E}}_{l,k \in \mathcal{K}_j}(\phi_{k,l});\ \tilde{\theta}_j = \mathop{\mathbb{E}}_{l,k \in \mathcal{K}_j}(\theta_{k,l}). \tag{12}$$

However, the phase shifters connected to antenna elements are controlled by b bits. Therefore, a beam can be steered in some specified direction only. The possible the possible steering directions can range from the set $\mathcal{F} = \{2\pi i/2^b | i = 0, \ldots, 2^b - 1\}$. Therefore, the optimal steering directions for beam j in azimuth and elevation plane are

$$\bar{\phi}_j = \mathop{\text{argmax}}_{\phi \in \mathcal{F}} |\phi - \tilde{\phi}_j|;\ \bar{\theta}_j = \mathop{\text{argmax}}_{\theta \in \mathcal{F}} |\theta - \tilde{\theta}_j|. \tag{13}$$

Therefore, the analog precoding matrix $\mathbf{A}$ of the hybrid precoder is of the form

$$\mathbf{A} = \{\mathbf{a}_1, \ldots, \mathbf{a}_{N_B^{k\text{-means}}}\} \in \mathbb{C}^{N_T \times N_B^{k\text{-means}}}. \tag{14}$$

Here $\mathbf{a}_j \in \mathbb{C}^{N_T \times 1}$ is the RF weight vector of j^{th} beam and is independent of frequency. For a beam steered at angle $(\bar{\phi}_j, \bar{\theta}_j)$ RF weights for the array are given by (15).

V. Subcarrier and Baseband Precoder Design with QoS Constraint

A. Problem formulation

In the proposed system model employing k-means clustering, the RF beams are steered in the direction of user clusters, thus rendering them non-orthogonal. Additionally, the practical radiation pattern of a beam consists of sidelobes. Therefore, the users in group j served by beam j will experience sidelobe interference from the sidelobes of beam $i \neq j$ where $j = \{1, 2, \cdots, N_B\}$.

Let $\mathbf{B}[n] = \text{diag}\{b_j[n]\} \in \mathbb{C}^{N_B \times N_B}$ and $\mathbf{s}[n] = \{s_j[n]\} \in \mathbb{C}^{N_B \times 1}\ \forall$ denote the UAV baseband precoder and unit energy transmit signal at n^{th} subcarrier, respectively. Here $b_j[n]$ and $s_j[n]$ denote the complex baseband weight and input signal, respectively, on n^{th} subcarrier of j^{th} RF unit. Then the received signal over n^{th} subcarrier at user k served by beam j can be written as

$$y_k[n] = \underbrace{\mathbf{h}_k[n]\mathbf{a}_j b_j[n] s_j[n]}_{\text{desired signal}} + \underbrace{\sum_{i=1, i\neq j}^{N_B} \mathbf{h}_k[n]\mathbf{a}_i b_i[n] s_i[n]}_{\text{inter-user interference}} + z_k[n] \tag{16}$$

where $z_k[n]$ is complex Gaussian noise with distribution $\mathcal{N}(0, \sigma^2)$. The baseband precoder minimizes the inter-user interference effect at the transmitter end. A receive beamforming weight equivalent to a equalizer minimizes the inter-user interference at the user. Let $u_k[n]$ denote the linear equalizer

$$\mathbf{a}_j = \begin{cases} e^{-j\frac{2\pi}{\lambda_c}\frac{f_n}{f_c}d'\sin\bar{\theta}_j\left[(m-1)\cos\bar{\phi}_j+(n-1)\sin\bar{\phi}_j\right]} & \forall n,m \in \left[\left(\sum_{i=1}^{j-1}\sqrt{N_i}\right)+1 : \sum_{i=1}^{j}\sqrt{N_i}\right], \\ 0 & \text{otherwise.} \end{cases} \tag{15}$$

of k^{th} user at n^{th} frequency. Then the estimated signal of user k is $\hat{y}_k[n] = u_k[n]^H y_k \ \forall k,n$. Subsequently, the signal-to-interference-plus-noise ratio $\Gamma_{k,j}[n]$ of k^{th} user over the n^{th} subcarrier served by beam j is represented as

$$\Gamma_{k,j}[n] = \frac{|\mathbf{h}_k\mathbf{a}_j b_j[n]|^2 G_r}{\frac{N_0 B}{N_c} + \sum_{i=1,i\neq j}^{N_B}|\mathbf{h}_k[n]\mathbf{a}_i b_i[n]|^2 G_r}. \tag{17}$$

Therefore, the data rate of k^{th} user over the n^{th} subcarrier in j^{th} beam is $r_{k,j}[n] = (B/N_c)\log_2(1+\Gamma_{k,j}[n])$.

In this work, we consider that the backhaul link operates at the same frequency as the fronthaul link. Since the backhaul link is aligned and narrow, we assume the UAV backhaul antenna panel gain $G_b \approx N_b G_0$ and the gNB backhaul antenna panel gain $G_g \approx N_g G_0$. Let R_k denote the instantaneous rate of a user k served by beam j, given by

$$R_k = \sum_{n=1}^{N_c}\pi_{k,j}[n] r_{k,j}[n] \tag{18}$$

where the variable $\pi_{k,j}[n] = 1$ if k^{th} user assigned n^{th} subcarrier on j^{th} beam; 0 otherwise. Moreover, the backhaul capacity should be at least equal to the fronthaul sum rate, i.e., $\sum_k R_k$. Then the required backhaul power is

$$P_B = \frac{2^{\sum_k R_k/B} - 1}{|h_B|^2 G_b G_g \text{PL}_B / N_0 B} \tag{19}$$

where h_B and PL_B are the small scale fading channel and pathloss of backhaul link, respectively. Thus the value of P_B is a function of the instantaneous fronthaul rate that depends on the precoding, subcarrier allocation, and P_T. Additionally, given a limit on total communication module power P_{limit}, from (6) the power available for fronthaul transmission is

$$P_T = \frac{P_{limit} - (N_B+1)P_{RF}}{1+\eta_{PA}} - P_B. \tag{20}$$

We optimize the subcarrier and baseband precoders to maximize the sum throughput with the specified QoS requirement R_0, given N_B and the accompanying RF precoder design. Therefore, the downlink sum rate optimization problem at the UAV is represented as

$$\begin{aligned} (\mathcal{P}1): \quad & \max_{\pi_{k,j}[n],\mathbf{B}} \sum_{j=1}^{N_B}\sum_{k\in\mathcal{K}_j}\left(\sum_{n=1}^{N_c}\pi_{k,j}[n]r_{k,j}[n]\right) \\ \text{s.t.} \quad & C11: \sum_{k=1}^{K_s}\pi_{k,j}[n] \leq 1, \ \forall n,j \\ & C12: \pi_{k,j}[n] \in \{0,1\}, \ \forall k,n,j \\ & C13: \sum_{n=1}^{N_c}\pi_{k,j}[n]r_{k,j}[n] \geq R_0 \ \forall k \\ & C14: \sum_{n=1}^{N_c}\text{Tr}(\mathbf{B}[n]\mathbf{B}[n]^H) \leq P_T. \end{aligned} \tag{21}$$

In each group in an epoch, the subcarriers are allocated only to a subset of users $k \in \mathcal{K}_j$ that are not in complete outage. We define k^{th} user to be in complete outage if with unit power $\max_{n\in\mathcal{N}_c}\{\Gamma_{k,j}[n]\} < \Gamma_{th}$. Here, Γ_{th} denote the threshold value. The above problem is non-convex since the objective function and constraint $C13$ are non-convex. $(\mathcal{P}1)$ can be solved used using alternating optimization method which iteratively solves for $\pi_{k,j}[n]$ while fixing $\mathbf{B}$ and P_T, and vice versa, until convergence is obtained. However, this is a computationally intensive procedure and may not guarantee convergence. Additionally, the constraint $C14$ requires optimization of P_T. This is because, as given in (20), P_T is a function of P_B that depends on user sum rate which in turn is an increasing function of P_T. Hence, P_B and P_T have positive covariance. As a result, to solve $\mathcal{P}1$ the value of P_T is estimated using golden-section search method such that sum rate is maximized while (20) holds. The starting value of P_T is chosen by assuming negligible power consumption in backhaul, i.e.,

$$P_T = P_{limit} - (N_B+1)P_{RF}/(1+\eta_{PA}). \tag{22}$$

B. Proposed subcarrier allocation and baseband precoder design

This subsection presents the proposed approach to find optimal subcarrier allocation, UAV baseband precoder design, and equalizer weights at the users to maintain QoS. The process is divided in two steps. Initially assuming zero inter-user interference, equal power per subcarrier, $\mathbf{B} = \sqrt{P_T/N_c N_B}\mathbf{I}_{N_B}$, and unity equalizers at users, subcarriers are allocated to the users to maximize the sum throughput while assuring minimum QoS to the users that are not in a complete outage. Next, baseband precoder and equalizer weights are estimated along with subcarrier reallocation in an iterative manner to maintain QoS. The baseband precoder and equalizers are designed by converting the sum rate maximization problem using weighted MMSE (WMMSE) precoder. The cost function is used to reallocate subcarriers.

1) Part 1: Initial subcarrier allocation: Given $\{\mathbf{A}, N_B\}$, fixing $\{P_T\}$, $\mathbf{B} = \sqrt{P_T/N_c N_B}\mathbf{I}_{N_B}$, and unity equalizers at users in $\mathcal{P}1$, we perform an initial subcarrier allocation to maximize the sum rate while satisfying minimum QoS rate requirements of all users assuming zero inter-beam interference. To solve this problem we use a sub-optimum approach leveraging the combination of direct search and external point search that yields a sub-optimal solution close to the optimal solution. In this, first the subcarriers are allocated to maximize the sum rate by relaxing $C13$. This gives a solution that is not from the feasible set but acts as the initial point for the search. Thereafter, the subcarrier allocation is adjusted on user-by-user basis to satisfy constraint $C13$. The steps involved in are:

(i) With the consideration of $\mathbf{B} = \sqrt{P_T/N_c N_B}\mathbf{I}_{N_B} \in \mathbb{C}^{N_B\times N_B}$ and zero inter-user interference, we calculate $r_{k,j}[n] \ \forall k,n,j$ using (17).

(ii) Because of zero inter-user interference assumption, subcarrier allocation in each beam is carried out independently. In beam j, each subcarrier is assigned to a user with the best channel condition. Hence, the optimal user assignment over n^{th} subcarrier in j^{th} beam is found as

$$\hat{k}_{n,j} = \underset{k\in\mathcal{K}_j}{\text{argmax}}\ r_{k,j}[n]\ \forall n, j. \tag{23}$$

As a result, $\pi_{\hat{k}_{n,j},j}[n] = 1$ and $\pi_{k,j}[n] = 0\ \forall k \neq \hat{k}_{n,j}$.

(iii) Let $\mathcal{K}'_j \subset \mathcal{K}_j$ represent the set of users that violate constraint $C13$ from step (ii). We employ the error minimization method to allocate subcarriers on a user-by-user basis to all users $k \in \mathcal{K}'_j$ to satisfy $C13$ (unless the user is in complete outage). The error function is defined for all $k \in \mathcal{K}'_j\ \forall n$ as [34]

$$E_{k,j}[n] = (r_{\hat{k}_{n,j},j}[n] - r_{k,j}[n])/r_{k,j}[n]$$

where $\hat{k}_{n,j}$ is the user that is initially assigned to n^{th} subcarrier on j^{th} beam from step (ii). The error is proportional to the reduction in overall sum rate.

(iv) The user $k \in \mathcal{K}'_j$ that has minimum error is allocated a subcarrier, i.e., $\tilde{n} = \underset{n}{\text{argmin}}\ E_{k,j}[n]$. It should be noted that during subcarrier reallocation, a subcarrier $\tilde{n}$ should not be reassigned to the user k if it violates the minimum rate requirements of the user originally allocated to $\tilde{n}$ subcarrier., i.e, if $R_{\hat{k}_{\tilde{n},j}} - r_{\hat{k}_{n,j},j}[\tilde{n}] < R_0$, where $R_{\hat{k}_{n,j}} = \sum_{n=1}^{N_c} \pi_{\hat{k}_{n,j},j}[n] r_{\hat{k}_{n,j},j}[n]$ is the rate of optimal user $\hat{k}_{n,j}$ over n^{th} subcarrier on j^{th} beam found using (23). If $R_k \geq R_0$ then $\mathcal{K}'_j = \mathcal{K}'_j/k$.

(v) Steps (iii) and (iv) are repeated until $\mathcal{K}'_j = \emptyset$ or subcarriers cannot be further re-assigned.

(vi) Steps (ii) and (v) are repeated for all $j = \{1, \ldots, N_B\}$.

Remark 1. *In case $|\mathcal{K}_j| > N_c$, only N_c among $|\mathcal{K}_j|$ users with best channel conditions are allocated subcarriers fulfilling their QoS rate requirements while the remaining $|\mathcal{K}_j| - N_c$ users are considered in outage in that epoch.*

2) Joint baseband precoding and subcarrier reallocation: Now we iteratively design UAV baseband precoder $\mathbf{B}$ and user equalizer weights $\mathbf{u}$ and reallocate the subcarriers. We begin with the knowledge of initial subcarrier allocation from section V-B1. Then at each iteration by relaxing C13 we estimate $\{\mathbf{B}, \mathbf{u}\}$ using WMMSE precoder to maximize the sum rate.

The steps to design baseband precoder design and equalizer weights using WMMSE are given in Algorithm 1. Let $k^*_{n,j}$ denote the optimal user assignment over subcarrier n on beam j. For fixed $(\mathbf{A}_{RF}, \{\pi_{k^*_{n,j},j}[n]\}_{\forall n,j})$, the optimal baseband precoders $\mathbf{B}$ and $\mathbf{u} = \{u_{k^*_{n,j},j}[n]\}_{\forall n,j}$ that maximizes total rate are found by solving the given problem

$$\begin{aligned}(\mathcal{P}2): \quad & \max_{\mathbf{u},\mathbf{B}} \sum_{j=1}^{N_B}\sum_{n=1}^{N_c} r_{k^*_{n,j},j}[n] \\ \text{s.t.} \quad & C21: \sum_{n=1}^{N_c} \text{Tr}(\mathbf{B}[n]\mathbf{B}[n]^H) \leq P_T\end{aligned} \tag{24}$$

Assuming Gaussian signaling, the rate of user $k^*_{n,j}$ assigned on n^{th} subcarrier beam in j is

$$r_{k^*_{n,j},j}[n] = \log_2(1 + Z_{k^*_{n,j},j}[n]^{-1} \left|\mathbf{h}_{k^*_{n,j}}[n]\mathbf{a}_j b_j[n]\right|^2) \tag{25}$$

where $Z_{k^*_{n,j},j}[n]$ is the noise covariance on n^{th} subcarrier from rest of the beams that is given by

$$Z_{k^*_{n,j},j}[n] = \sigma^2 + \sum_{i\neq j} \left|\mathbf{h}_{k^*_{n,j}}[n]\mathbf{a}_i b_i[n]\right|^2. \tag{26}$$

The MMSE receiver $u_{k^*_{n,j},j}[n]$, is given as [35]

$$u_{k^*_{n,j},j}[n] = \frac{\mathbf{h}_{k^*_{n,j}}[n]\mathbf{a}_j[n]b_j[n]}{Z_{k^*_{n,j},j}[n] + \left|\mathbf{h}_{k^*_{n,j}}[n]\mathbf{a}_j[n]b_j[n]\right|^2}. \tag{27}$$

Applying MMSE receiver, the error at user $k^*_{n,j}$ is

$$\begin{aligned} e_{k^*_{n,j},j}[n] &= \mathbb{E}\Big[(u_{k^*_{n,j},j}[n]y_{k^*_{n,j},j}[n] - x_j[n]) \\ &\quad \times (u_{k^*_{n,j},j}[n]y_{k^*_{n,j},j}[n] - x_j[n])^H\Big] \\ &= \left(1 + Z_{k^*_{n,j},j}[n]^{-1}\left|\mathbf{h}_{k^*_{n,j}}[n]\mathbf{a}_j b_j[n]\right|^2\right)^{-1}. \end{aligned} \tag{28}$$

Now we transform the sum rate maximization problem $\mathcal{P}2$ into weighted sum-rate mean square error (WMMSE) minimization problem as [35]

$$\begin{aligned}(\mathcal{P}3): \quad & \min_{\mathbf{w},\mathbf{u},\mathbf{B}} \sum_{j=1}^{N_{RF}}\sum_{n=1}^{N_c} \left(w_{k^*_{n,j},j}[n]e_{k^*_{n,j},j}[n] - \log_2(w_{k^*_{n,j},j}[n])\right) \\ \text{s.t.} \quad & C31: \sum_{n=1}^{N_c} \text{Tr}(\mathbf{B}[n]\mathbf{B}[n]^H) \leq P_T.\end{aligned} \tag{29}$$

Here, $w_{k^*_{n,j},j}[n]$ denote the positive weight associated with the $k^*_{n,j}$ user assigned on n^{th} subcarrier in j^{th} RF unit. Problem $\mathcal{P}3$ is convex in all the optimization variables. Hence, the Lagrangian of $\mathcal{P}3$ is given as

$$\begin{aligned}\mathbf{L} = &\sum_{j=1}^{N_{RF}}\sum_{n=1}^{N_c} \left(w_{k^*_{n,j},j}[n]e_{k^*_{n,j},j}[n] - \log w_{k^*_{n,j},j}[n]\right) \\ &- \lambda\left(\sum_{n=1}^{N_c} \text{Tr}(\mathbf{B}[n]\mathbf{B}[n]^H) - P_T\right)\end{aligned} \tag{30}$$

where λ is the positive Lagrangian multiplier. Therefore, solving for one variable by taking partial derivative of (30) with respect to that variable, while keeping other variables fixed, gives a local optimal. Therefore, the optimal weights are given as

$$w_{k^*_{n,j},j}[n] = \frac{1}{e_{k^*_{n,j},j}[n]}. \tag{31}$$

Substituting the values of the equalizers $u_{k^*_{n,j},j}[n]$, error $e_{k^*_{n,j},j}[n]$, and weights $w_{k^*_{n,j},j}[n]$ in $\mathcal{P}3$ we have the equivalence as

$$\begin{aligned}(\mathcal{P}4): \quad & \max_{\mathbf{B}} \sum_{j=1}^{N_{RF}}\sum_{n=1}^{N_c} \log_2\left(1 + \frac{\left|\mathbf{h}_{k^*_{n,j}}[n]\mathbf{a}_j b_j[n]\right|^2}{\sigma^2 + \sum_{i\neq j}\left|\mathbf{h}_{k^*_{n,j}}[n]\mathbf{a}_i b_i[n]\right|^2}\right) \\ \text{s.t.} \quad & C31.\end{aligned} \tag{32}$$

where $\mathcal{P}4$ is convex in $b_j[n]\ \forall j,n$. Consequently, we solve it using KKT to obtain

$$b_j^*[n] = \frac{w_{k^*_{n,j},j}[n] u^H_{k^*_{n,j},j}[n] \mathbf{h}_{k^*_{n,j}}[n] \mathbf{a}_j}{\nu + |u^H_{k^*_{n,j},j}[n]|^2 \sum_i w_{k^*_{n,j},i}[n] |\mathbf{h}_{k^*_{n,j}}[n] \mathbf{a}_i|^2} \quad (33)$$

where ν is the Lagrangian multiplier corresponding to C31. Substituting value of $b_j^*[n]$ in C31, we have

$$\sum_{n=1}^{N_c} \sum_{j=1}^{N_{RF}} \frac{\left| w_{k^*_{n,j},j}[n] u^H_{k^*_{n,j},j}[n] \mathbf{h}_{k^*_{n,j}}[n] \mathbf{a}_j \right|^2}{\left(\nu + |u^H_{k^*_{n,j},j}[n]|^2 \sum_i w_{k^*_{n,j},j}[n] |\mathbf{h}_{k^*_{n,j}}[n] \mathbf{a}_i|^2 \right)^2} \leq P_T. \quad (34)$$

Here, (34) is a decreasing function of ν and is solved using numerical methods. Therefore, if $\sum_{n=1}^{N_c} \text{Tr}\{\mathbf{B}_{\nu=0}[n] \mathbf{B}_{\nu=0}[n]\}^H \leq P_T$, then $\mathbf{B}^*[n] = \mathbf{B}_{\nu=0}[n]$; otherwise ν^* is found using bisection search. The steps to find baseband precoder design and equalizer of user are given in Algorithm 1.

It is notable that solving for $\{\mathbf{B}, \mathbf{u}\}$ using Algorithm 1 might violate minimum QoS rate constraint C13 of some users. The use of penalty-based WMMSE precoder design optimization is one technique to ensure C13 [36]. However, this approach has an extremely slow convergence rate. Therefore, we propose to jointly reallocate subcarriers to users along with the re-design of $\{\mathbf{B}, \mathbf{u}\}$ design such that QoS of users is maintained. The steps are listed in Algorithm 2, which has a faster rate of convergence.

In Algorithm 2 we traverse each subcarrier one-by-one. On n^{th} subcarrier, we find the set of users $\mathcal{K}_n = \{k^*_{n,j} | R_{k^*_{n,j}} > R_0,\ \forall j\}$. If $\mathcal{K}_n \neq \emptyset$ then we find the cost function at n^{th} subcarrier defined as

$$c_{k^*_{n,j}}[n] = R_{k^*_{n,j}} - r_{k^*_{n,j},j}[n]\ \forall k^*_{n,j} \in \mathcal{K}_n. \quad (35)$$

Thereafter, we find the user that has the highest cost using is selected using the relation

$$k'_n = \underset{k^*_{n,j} \forall j}{\text{argmax}}\ c_{k^*_{n,j}}[n]. \quad (36)$$

For the user k'_n we set $\pi_{k'_n,j}[n] = 0$ if and only if $c_{k^*_{n,j}} > R_0$; otherwise go to next subcarrier. We also update $\mathcal{K}_n, R_k$ and re-design $\{\mathbf{B}[n], \mathbf{u}[n]\}_{\forall n}$ before moving to the next subcarrier. This procedure is repeated over all the N_c subcarriers till the convergence is achieved. The stopping criteria of this algorithm is defined when the $R_k > R_0\ \forall k$ or each subcarrier has at most one user assigned to it and hence, further subcarrier reallocation is not possible. If all the subcarriers have maximum one user assigned on it and $\mathcal{K}_n \neq \emptyset$, then the process is stopped even though $C13$ is not fulfilled for some of the users.

Remark 2. *In Algorithm 2, the WMMSE method to estimate $\{\mathbf{B}[n], \mathbf{u}[n]\}_{\forall n}$ is executed at most N_B times per subcarrier. So, $\{\mathbf{B}[n], \mathbf{u}[n]\}_{\forall n}$ are estimated a maximum of $N_c N_B$ times.*

C. Complexity analysis

The complexity of k-means clustering for K users is $\mathcal{O}(K^2)$. The subcarrier allocation design in Section V-B1 requires $\mathcal{K}_j N_c$ comparisons in step (ii) , $(\mathcal{K}_j - 1)N_c$ additions and $(\mathcal{K}_j - 1)N_c$ multiplications in step (iii) to find error function, and $2N_c^2$ comparisons for subcarrier allocation in step (iv). Steps (ii)-(iv) are executed for $j = \{1, \ldots, N_B\}$. Therefore, the total complexity of subcarrier allocation is $\mathcal{O}(\sum_{j=1}^{N_B}(2(\mathcal{K}_j - 1)N_c + \mathcal{K}_j N_c + 2N_c^2))$. The dominant computational term in WMMSE precoder design results from the multiplication of $\mathbf{h}_{k^*_{n,j},j}[n]$ and $\mathbf{a}_j^*$ terms for all the beams. Let ζ_I denote the iterations required for convergence of Algorithm 1. Then the total complexity ofr WMMSE precoder is $\mathcal{O}(\zeta_\eta \zeta_I N_T N_B N_c^2)$. Further, in Algorithm 2 the number of iterations of convergence is limited to $\zeta_P = N_c N_B$. Therefore, the overall complexity of proposed joint subcarrier and baseband precoder design in Algorithm 2 is $\mathcal{O}(\zeta_P \zeta_I N_T N_B N_c^2)$.

Algorithm 1 WMMSE precoder

Input: $N_{RF}, \pi_{k^*_{n,j},j}[n]^*, \mathbf{A}_{RF}, \mathbf{h}_{k^*_{n,j}}[n]\ \forall k,j,n$
Output: $\mathbf{B}[n]$ and $u_{k^*_{n,j},j}[n]$
Initialize $\mathbf{B}[n] = \mathbf{I}_{N_B}\sqrt{P_T/(N_c N_{RF})}$
do
  Find $u_{k^*_{n,j},j}[n]$ using (27) $\forall j,n$
  Find $w'_{k^*_{n,j},j}[n] \leftarrow w_{k^*_{n,j},j}[n]$ using (31) $\forall j,n$
  Find ν using (34)
  Find $b_j[n]$ using (33) $\forall j,n$
  Update $w_{k^*_{n,j},j}[n]$ (31) $\forall j,n$
while $\left|\sum_j \text{logdet}(\sum_n w'_{k^*_{n,j},j}[n]) - \text{logdet}(\sum_n w_{k^*_{n,j},j}[n])\right| \leq \epsilon$

Algorithm 2 Joint subcarrier allocation and baseband precoder design with QoS constraints

Input: Analog precoder, N_c, $\{\mathbf{h}_k[n]\}_{\forall n,k}$, N_{RF}, R_0, K, P_T
Output: $\{\pi_{k,j}[n]\}^*, \mathbf{B}[n]$, $u_{k^*_{n,j},j}[n]\ \forall k,n,j$
Initially assume zero inter-beam interference
Initialize $\mathbf{B}[n] = \mathbf{I}_{N_B}\sqrt{P_T/(N_c N_{RF})}$
Allocate subcarriers using steps in V-B1
Find $\mathbf{B}[n]$ and $u_{k^*_{n,j},j}[n]$ using Algorithm 1
Update $r_{k,j}[n]\ \forall b$ and $R_k\ \forall k$
do
  for $n = 1$ to N_c **do**
    Find $\mathcal{K}_n = \{k^*_{n,j} | R_{k^*_{n,j}} > R_0,\ \forall j\}$
    while $\mathcal{K}_n \neq \emptyset$ **do**
      Find $c_{k^*_{n,j}}\ \forall j$ using (35)
      Find k'_n using (36)
      $\pi_{k'_n,j}[n] \leftarrow 0$ iff $c_{k^*_{n,j}} > R_0$
    end while
    Update $r_{k,j}[n]\ \forall k,j,n$ and $R_k\ \forall k$
    Re-design $\mathbf{B}[n]$ and $u_{k^*_{n,j},j}[n]\ \forall j$ using Algorithm 1
  end for
while stopping criteria is satisfied

VI. UAV Solar Panel Design

In addition to optimal user grouping and baseband signal processing, the UAV hardware also impacts the overall energy efficiency of the system. To sustain UAV operation for a longer duration we consider solar energy harvesting. When there is no solar insolation (eclipse mode), the UAV payload consists of a battery that supplies backup power. When solar insolation exceeds the minimum needed level, the battery is recharged using solar panels. Let the solar insolation is available for a

duration of T_s hours. During eclipse mode of T_c duration the battery sustains the UAV operation. It is worth noticing that solar panel has weight that increases UAV hovering power thereby reducing the energy efficiency of the system. This section describes the design of the UAV solar panel for a sustainable long-term UAV operation.

The solar photovoltaic (PV) system consists of a PV array composed of solar panels connected in series and parallel combinations and a maximum power point tracker between the battery and the PV array to regulate the solar energy. The foremost requirement to design a PV system is to estimate the total load requirement. During the the solar insolation period T_s, the PV system charges the battery as well as supports the UAV operation. Let C_B denote the battery capacity in amp-hour and μ_c be the battery charging rate. Then, the total watt-hours requirement from solar panels is

$$T_{WH} = C_B/\mu_c + (P_C + P_{hover})T_s. \tag{37}$$

Thus, UAV hovering power consumption P_{hover} from (8) is

$$P_{hover}(W_{UAV}) = \frac{W_{UAV}^{3/2}}{\sqrt{2g\alpha'\rho\beta}} \tag{38}$$

where the total UAV weight given as

$$W_{UAV} = (W_B + W_{PV} + W_0) \text{ kg} \tag{39}$$

Here, W_B is battery weight, W_{PV} is PV array weight, and W_0 is the sum of weight of the different components of UAV hardware units like servomotor, engine, and RF circuit as listed in Table III. It is notable that P_{hover} is function of W_{PV}. On the other hand, the value of W_{PV} depend on P_{hover}. Therefore, estimating solar panel size is an iterative process which is presented in Algorithm 3. The calculation of battery weight W_B and solar panel weight W_{PV} follows.

A. Battery weight

During eclipse mode, the total UAV power consumption is $P_{Tot} = P_C + P_{hover}$ W. Let μ_d denote the battery discharging rate, V_u denote the operating voltage. Then, for the battery to support UAV operation during eclipse mode we have

$$C_B\mu_d V_u = T_c P_{Tot} \Rightarrow C_B \quad = T_c P_{Tot}/(\mu_d V_u). \tag{40}$$

A battery of capacity C_B is made up of small cells of capacity C_b, i.e., $C_B = \mathcal{N}_b C_b$, where $\mathcal{N}_b$ is the number of cells. With per unit battery weight W_b, the total battery weight is

$$W_B = m_2 g = \mathcal{N}_b W_b. \tag{41}$$

B. Solar panel weight

Number of solar cells in parallel N_{parall} depends on the voltage rating of a solar cell V_s, voltage rating of the battery V_b, and the voltage rating of the UAV V_u. Therefore,

$$\mathcal{N}_{parall} = \lceil \max(V_b, V_u)/V_s \rceil \tag{42}$$

The number of solar cells in series $\mathcal{N}_{ser}$ depends on UAV load and the available radiation. Let the average radiation level per solar cell during solar insolation hours be I_s W/m^2/hr, charging efficiency of PV array be η_s, and per unit area of a solar cell be A_s. Then, the number of solar panels in series N_{ser} required to satisfy estimated demand is found as

$$\mathcal{N}_{ser} = \left\lceil \frac{\text{Total watt-hour required}}{\text{Watt-hour produced per cell}} \right\rceil = \left\lceil \frac{T_{WH}}{A_s I_s T_s \eta_s} \right\rceil. \tag{43}$$

Therefore, if W_S is the unit solar cell weight, then the total weight of the PV array is

$$W_{PV} = m_3 g = \mathcal{N}_{ser}\mathcal{N}_{prarall} W_S. \tag{44}$$

Table III: UAV design specifications

Component	Quantity	Unit weight
Li-ion battery (W_b)	N_b	0.0465 kg [37]
Solar cell (W_S)	$N_{ser} \times N_{parall}$	0.0065 kg [38]
Servomotor	4	0.0098 kg [39]
Main engine	1	0.055 kg [39]
RF circuit	2	0.026 kg [39]

VII. Results and Discussion

This section presents the numerical results and discussion of the various results to study the proposed system model. The results are generated in MATLAB using Monte Carlo simulations. Users are distributed using the Cox point process over a circular area of radius $\mathcal{R} = 100$ m. The value of other system parameters considered in the system simulation setup are given in Table IV. The analysis for both mmWaves and sub-6 GHz range are carried out. The superscript 'mm' denotes the mmWave parameter, and the 'sub' denotes sub-6 GHz parameters.

Algorithm 3 Solar panel design

1: Input: $\mu_d, \mu_c, \eta_s, T_c, T_s$, $\mathcal{N}_b$, and C_B
2: Output: $\mathcal{N}_b$ and $\mathcal{N}_{ser}$
3: Initialize $\mathcal{N}_{ser} = 1, P_0 = \infty$, and $P_{hover} = 0.2818$
4: **while** $|P_{hover} - P_0| < 0.0001$ **do**
5: $\quad P_0 \leftarrow P_{hover}$
6: $\quad$ Find N_{ser} using (43)
7: $\quad$ Calculate W_{PV}
8: $\quad$ Update P_{hover} by using (39) and (44) in (38)
9: **end while**

Table IV: Simulation parameters

Parameter	Value	Parameter	Value
N_c	64	K	30
f_c	5 GHz, 28 GHz	N_0	-174 dBm/Hz
B^{mm}	400 MHz	B^{sub}	20 MHz
N_t^{mm}	64×64	N_t^{sub}	12×12
N_b^{mm}	8×8	N_b^{sub}	2×2
N_g^{mm}	8×8	N_g^{sub}	2×2
η_{PA}^{mm}	47% [31]	η_{PA}^{sub}	60%[40]
κ^{mm}	12.6 dB	κ^{sub}	0 dB
h_U	100 m	$d_{UAV-gNB}$	400m
h_{gNB}	30 m	ς	500 [41]
R_0	$\{1, 2, 5, 10, 20\}$ Mbps	N_B^{max}	$64/N_B$
ξ	0.3 [41]	ω	15 [41]
α'	4 [24]	β	0.045 m^2 [24]
ρ	1.225 kg/m^3 [24]	C_b	2000 mAh
A_s	125×125 mm^2	I_s	1.37 KWH/m^2
μ_d	80%	μ_c	20%
V_s	6 V	V_u	12 V
V_b	12 V	η_s	22%

A. Sectorization versus k-means clustering at mmWaves

Let $\sigma_{spread} = 360^o/\chi$ represent the angular spread of the users over $\mathcal{A}$, where, $\chi \in (1, 360)$ is the skewness parameter. When $\chi = 1$, the users are uniformly distributed over 360^o; when $\chi = 360$ the users are confined to an angular area of 1^o and the skewness is maximum.

Further, for serving a number of users which is greater than the number of RF chains at the UAV, we compare the proposed user grouping using k-means with the sector based user grouping scheme in [17]. To form identical sectors, we the place UAV at the center of the area $\mathcal{A}$. In [17] it is shown that the lateral projection of a 3D beam can be approximated close to a sector formation. Therefore, for the sectorization of an area, we consider that each RF beam covers a single sector. Subsequently, the area $\mathcal{A}$ having total K users is divided into sectors equal to the number of RF beams $N_B = N_B^{\text{sector}}$ at the UAV, as shown in Fig. 2. Therefore, the half-power azimuth beamwidth Φ and half-power elevation beamwidth Θ are equal for all the beams and are given as

$$\Phi = \frac{360^o}{N_B^{\text{sector}}};\ \Theta \quad = \tan^{-1}\left(\frac{\mathcal{R}}{h_U}\right) - \tan^{-1}\left(\frac{\mathcal{R}-\mathcal{R}_0}{h_U}\right) \tag{45}$$

where $\mathcal{R}$ is radius of area $\mathcal{A}$ and $\mathcal{R}_0$ is the interior radius beyond which no beam coverage can be extended, as shown in Fig. 2. Hence, the $\sqrt{N_T}\times\sqrt{N_T}$ UPA is divided into N_B^{sector} non-overlapping subarrays of equal dimensions $\sqrt{N_e}\times\sqrt{N_a}$, where N_e and N_a denote the number of active antenna elements in elevation and azimuth plane, respectively. The values of N_e and N_a are determined as follows [33]:

$$\begin{aligned} N_e &= \min\left(\left\lceil\frac{2.782}{\pi\sin(\Theta)\cos(\tan^{-1}(d_k/h_U))}\right\rceil, \frac{N_T}{N_B^{\text{sector}}}\right) \\ N_a &= \min\left(\left\lceil\frac{2.782}{\pi\sin(\Phi)\cos(\tan^{-1}(d_k/h_U))}\right\rceil, \frac{N_T}{N_B^{\text{sector}}}\right). \end{aligned} \tag{46}$$

Consequently, steering directions of j^{th} beam in azimuth and elevation plane, respectively, are

$$\bar{\phi}_j = \frac{1}{2}\frac{360^o}{\Phi} + (j-1)\frac{360^o}{\Phi};\ \bar{\theta}_j \quad = \tan^{-1}\left(\frac{\mathcal{R}/2}{h}\right). \tag{47}$$

The analog precoding matrix $\mathbf{A}$ of the hybrid precoder is obtained by substituting these values in (15).

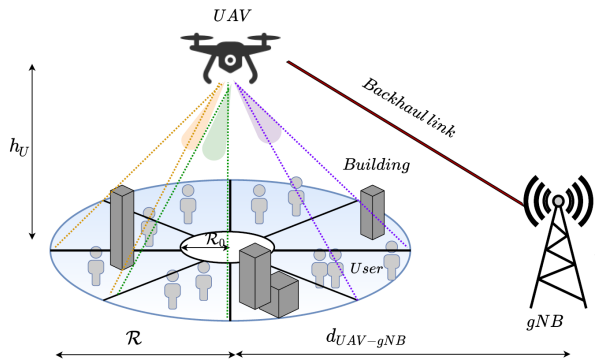

Figure 2: Illustration of user grouping by partitioning the area into $N_B^{\text{sector}} = 8$ sectors with each sector served by one RF beam.

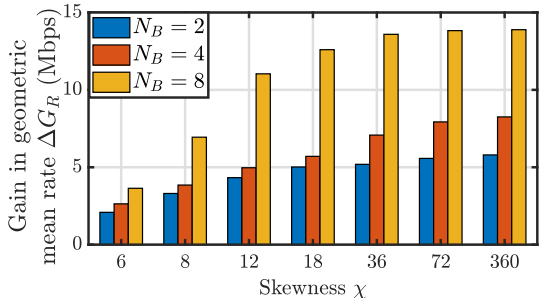

Figure 3: Plot of gain in geometric mean rate ΔG_R achieved by using k-means clustering over sectoring approach at mmWaves, given $P_{limit} = 5$ W and $N_B = N_B^{k\text{-means}} = N_B^{\text{sector}}$.

Let $\Delta G_R = G_R^{k\text{-means}} - G_R^{\text{sector}}$, where $G_R^{k\text{-means}}$ and G_R^{sector} respectively denote the geometric mean rate achieved with user grouping using k-means clustering and sectoring method. Geometric mean is given as $G_R = (\prod_{k=1}^{K} R_k)^{(1/K)}$.

Fig. 3 shows the variation of ΔG_R as a function of skewness parameter χ for different number of RF units N_B at the UAV. We observe that the value of ΔG_R increases with skewness since all of the users are concentrated over a smaller area. In the sectoring approach, the closely located users are served by number of beams $N_B' < N_B$ that have users in corresponding sectors. Therefore, it is not able to exploit full spatial multiplexing gain. On the other hand, the proposed user grouping with k-means clustering uses full degree of spatial multiplexing by dividing the users into the available number of beams. It is notable that, in k-means clustering the number of beams N_B decides total number of user groups, whereas in sectoring N_B decides the total number of sectors. Moreover, the adjustable beamwidth and beam steering with k-means clustering method allows to direct maximum energy and beam towards the users to maximize the sum rate. Thus, sectoring approach is not suitable for mmWave UAV communications.

B. Performance of the proposed joint subcarrier and baseband precoder algorithm

We compare the performance of the proposed joint subcarrier optimization design method, named as 'Proposed based design', over a benchmark method, which we call 'Penalty based design' [36]. In penalty based method subcarrier allocation and baseband precoder design occurs separately. Subcarrier allocation occurs using error based method as given in Section V-B1, and baseband precoder and equalizers are estimated using penalty based WMMSE optimization to maintain QoS. Penalty based design optimizes the baseband precoder such that it increases the rate of all users that have $R_k < R_0$ while decreasing the rate of users having $R_k > R_0$, so that the sum rate is maximized and the users in bad channel conditions achieve $R_k > R_0$. In contrast, joint subcarrier and baseband method (Algorithm 2) achieves QoS by removing a user k_n' (cf. (36)) that has $R_k \gg R_0$ on a subcarrier and allocating it to another user. Therefore, as shown in Fig. 4(a), joint subcarrier and baseband method results in proportional rate allocation among the users. Furthermore, as shown in

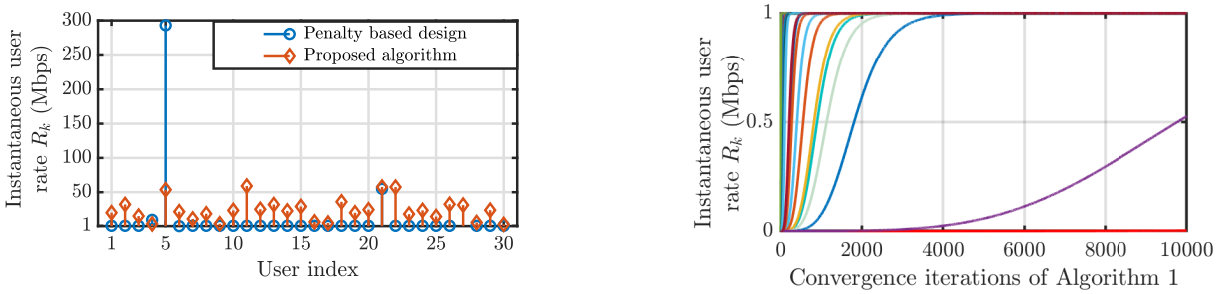

Figure 4: (a) Comparison of user rates achieved with proposed joint subcarrier and baseband design algorithm and penalty based design algorithm at mmWaves. (b) Illustration of the convergence of rate of users with penalty based design algorithm. Here, rate convergence of only those users is shown that initially had $R_k < R_0$.

Fig. 4(b), the number of iterations required for convergence of WMMSE precoder for penalty based design is quite high.

Besides, we first designs an RF precoder followed by joint subcarrier allocation and baseband precoder optimization. In contrast, works in the contemporary literature [42] first assign subcarriers and then schedule users using joint RF and baseband precoding to maximize sum throughput. Therefore, as a benchmark comparison we consider a system in which users are assigned subcarriers while meeting a minimum QoS constraint, and then RF and baseband precoders are optimized to minimize inter-user interference. Additionally, after precoding optimization power allocation is adjusted to maintain user QoS [15]. Fig. 5 shows that our proposed subcarrier allocation and precoding scheme offers a significantly higher G_R than the benchmark scheme over different values of χ. This is because in a benchmark system, the user with the best channel receives the maximum rate while the rest of the users receive the minimum rate, resulting in poor user fairness G_R.

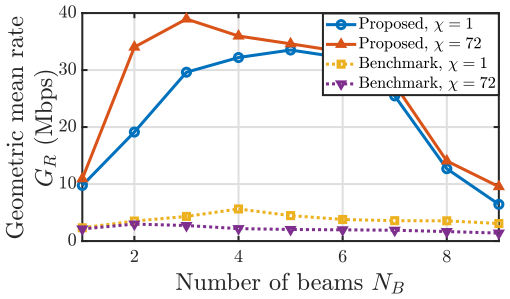

Figure 5: Performance comparison of the proposed subcarrier and precoder algorithm over the benchmark scheme [15] at mmWaves, given $P_{limit} = 5$ W.

C. Optimal N_B selection at mmWaves

As the number of beams increases, the power per beam decreases, and the RF power waste increases as given by (6). On the other hand, an increasing number of beams allows enhanced spatial multiplexing and narrow beams of higher directivity to cover the same set of users. As a result, the power requirements for UAVs and the achievable rates at mmWaves depend on N_B. Given P_{limit}, G_R is a concave function of N_B, as seen in Fig. 6. Thus, there exists an optimal number of beams that provide the best performance while ensuring that all users receive minimum rate support. We estimate optimal N_B^* in this paper by solving $\mathcal{P}1$ for different values of N_B. The value of N_B determines the number of user groups that can be formed and the RF precoder design that accompanies it, as discussed in Section IV. Subcarrier allocation and baseband precoder are designed as described in Section V-B for each value of N_B. Furthermore, we investigate the optimal number of beams selection at UAV using the geometric mean rate measure. The choice of N_B is also influenced by R_0. The value N_B^* drops as R_0 is increased.

Further, Fig. 7 shows that for a given value of N_B, the value of G_R increases as P_{limit} increases, which is quite intuitive. On the other hand, the optimal N_B^* is a non-linear function of P_{limit}. To this end, operating at the optimal number of RF units N_B^* for maximum performance gain is crucial for a long-term UAV operation.

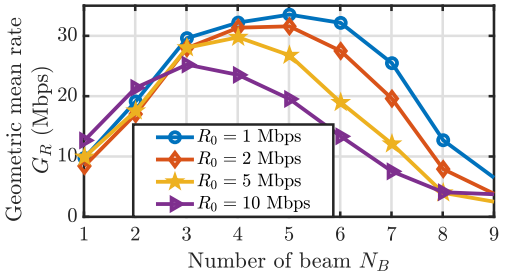

Figure 6: Illustration of geometric mean rate $\bar{R}$ as a function of number of beams N_B at mmWaves, given $P_{limit} = 5$ W, and $\chi = 1$.

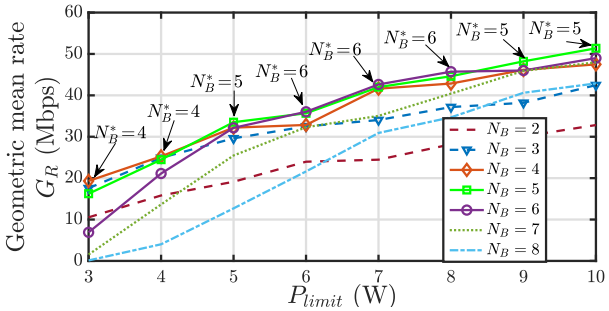

Figure 7: Plot of optimal N_B^* value as a function of available power P_{limit} for transmission module at UAV at mmWave range for $\chi = 1$.

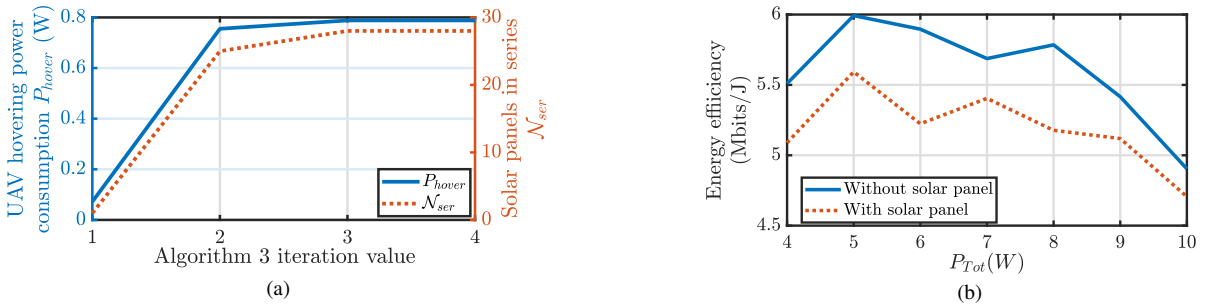

Figure 8: (a) Convergence of P_{hover} and $\mathcal{N}_{ser}$ when $P_{Tot} = 5$ W. (b) Illustration of energy efficiency of UAV with and without considering solar panels weight optimization.

D. Analysis of solar panel design at mmWaves

We also investigate the solar design aspects for a comprehensive view. As discussed in Section VI, the weight of a UAV increases with the number of solar cells, thus requiring more hovering power that corresponds to an increased solar panel size to sustain UAV operation. This is illustrated in Fig. 8 (a). We set $P_{Tot} = 5$ W, $T_s = 8$ hours, $T_c = 16$ hours for this simulation result, and the remainder of the design parameters are listed in Table IV. Fig. 8(b) shows the reduction in energy efficiency during eclipse mode because of additional weight of solar panel that increase P_{hover}, and hence resulting in reduced power available for the communication module. The curves in Fig. 8(b) are not smooth because the number of solar panels is an integer variable. Also, as shown in Fig. 8(b) UAV is energy efficient when it is operated at $P_{Tot} = 5$ W.

E. UAV communication performance comparison at sub-6 GHz versus at mmWaves

We also study the UAV performance and power requirements at the sub-6 GHz range for a comprehensive analysis. In simulations, we keep same antenna aperture for both the sub-6 GHz and mmWave systems. Hence, when $N_t^{mm} = 64 \times 64$ at mmWaves then $N_t^{mm} = 12 \times 12$. Also, 3GPP new radio (NR) defines a sector of $60^o \sim 65^o$ beamwidth in sub-6 GHz range. Therefore, in this work we consider $N_B^{sub} = 6$.

Notably, higher frequencies allow packaging of many antenna elements, thereby providing high beam gain and reduced transmit power. Moreover, a dedicated antenna panel with a large number of antenna elements is used at mmWaves to generate a pointed backhaul link. Along with that, mmWave operation offers bandwidth of around 400 MHz. As a result, the backhaul power at mmWaves is significantly less, on the order of mW. Consequently, more power is available for fronthaul transmission. In contrast, sub-6 GHz allows a small number of antenna elements resulting in low beam gain and thus, requiring high transmit power. Additionally, sub-6 GHz requires high power in backhaul P_B (Fig. 9) and thus reduced power available for fronthaul communication. Therefore, as shown in Fig. 9, the geometric mean rate G_R is higher at mmWaves than at sub-6 GHz range for the same power budget P_{limit}. Further, the value of P_B limits the overall fronthaul rate at sub-6 GHz. For example, when the total backhaul rate is 0.4 Gbps in sub-6 GHz range, P_B is as high as 8.45 W.

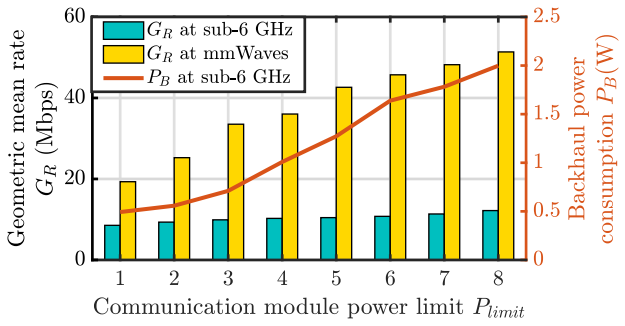

Figure 9: Comparison of $\bar{R}$ at sub-6 GHz and mmWaves at the UAV as a function of P_{limit} and illustration of P_B at sub-6 GHz. Here, $\chi = 1$, $R_0 = 1$ Mbps, $N_B^{sub} = 6$, and $N_B^{mm} = N_B^*$ (the optimal value that gives best performance at mmWaves).

VIII. Conclusion

This paper has demonstrated that low-altitude UAVs serving multiple users via OFDMA at mmWaves offer more than double the rates achieved at sub-6 GHz frequency for the same UAV power budget. This gain is due to increased gain from large antenna arrays and high bandwidth at mmWaves. It is also shown that grouping users using k-means clustering and adjusting beam coverage to target maximal radiation on the users is superior to sectorizing the area from both rate and energy efficiency perspective.

Accordingly, an RF precoder for the sub-array hybrid precoder architecture is designed. A combined subcarrier and baseband precoding technique is also proposed for the sub-array hybrid precoding architecture. It has a faster convergence rate and provides fair rate allocation to the users while meeting the minimum rate guarantee. To design baseband beamforming weights and equalizers, WMMSE method has been used to reduce inter-beam interference. It is also verified that with a given power budget, increasing the number of RF chains does not necessarily increase the system performance as the associated power waste in the RF circuitry increases. Moreover, the number of beams should be optimized for a sustainable operation for energy-constrained UAV-assisted communications at mmWaves. Finally, aiming at long-term UAV-assisted communications at mmWaves, the battery capacity and solar panel have been jointly optimized for the solar-powered UAV acting as an ambient powered 3D wireless base station.

REFERENCES

[1] 3GPP. (2019) Unmanned Aerial Systems (UAS) Support in 3GPP; Stage 1 – Rel. 17. TS 22.125.

[2] N. Kato, Y. Kawamoto, A. Aneha, Y. Yaguchi, R. Miura, H. Nakamura, M. Kobayashi, T. Henmi, O. Akimoto, Y. Kamisawa *et al.*, "Air-ground heterogeneous networks for 5G and beyond via integrating high and low altitude platforms," *IEEE Wireless Commun.*, vol. 26, no. 6, pp. 149–155, 2019.

[3] L. Zhang, H. Zhao, S. Hou, Z. Zhao, H. Xu, X. Wu, Q. Wu, and R. Zhang, "A survey on 5G millimeter wave communications for UAV-assisted wireless networks," *IEEE Access*, vol. 7, pp. 117 460–117 504, 2019.

[4] W. Yi, Y. Liu, E. Bodanese, A. Nallanathan, and G. K. Karagiannidis, "A unified spatial framework for UAV-aided mmWave networks," *IEEE Trans. Commun.*, vol. 67, no. 12, pp. 8801–8817, 2019.

[5] C. Qiu, Z. Wei, Z. Feng, and P. Zhang, "Backhaul-aware trajectory optimization of fixed-wing UAV-mounted base station for continuous available wireless service," *IEEE Access*, vol. 8, pp. 60 940–60 950, 2020.

[6] X. Jiang, M. Sheng, N. Zhao, C. Xing, W. Lu, and X. Wang, "Green UAV communications for 6G: A survey," *Chinese J. Aeronaut.*, 2021.

[7] M. Mozaffari, W. Saad, M. Bennis, Y.-H. Nam, and M. Debbah, "A tutorial on UAVs for wireless networks: Applications, challenges, and open problems," *IEEE Commun. Surveys Tuts.*, vol. 21, no. 3, pp. 2334–2360, 2019.

[8] Y. Kawamoto, H. Nishiyama, N. Kato, F. Ono, and R. Miura, "Toward future unmanned aerial vehicle networks: Architecture, resource allocation and field experiments," *IEEE Wireless Commun.*, vol. 26, no. 1, pp. 94–99, 2019.

[9] C. Zhang, W. Zhang, W. Wang, L. Yang, and W. Zhang, "Research challenges and opportunities of UAV millimeter-wave communications," *IEEE Wireless Commun.*, vol. 26, no. 1, pp. 58–62, 2019.

[10] W. Khawaja, I. Guvenc, D. W. Matolak, U.-C. Fiebig, and N. Schneckenburger, "A survey of air-to-ground propagation channel modeling for unmanned aerial vehicles," *IEEE Commun. Surveys Tuts.*, vol. 21, no. 3, pp. 2361–2391, 2019.

[11] S. Kang, M. Mezzavilla, A. Lozano, G. Geraci, W. Xia, S. Rangan, V. Semkin, and G. Loianno, "Millimeter-wave UAV coverage in urban environments," pp. 1–6, 2021.

[12] G. Fontanesi, A. Zhu, and H. Ahmadi, "Outage analysis for millimeter-wave fronthaul link of UAV-aided wireless networks," *IEEE Access*, vol. 8, pp. 111 693–111 706, 2020.

[13] M. Gapeyenko, V. Petrov, D. Moltchanov, S. Andreev, N. Himayat, and Y. Koucheryavy, "Flexible and reliable UAV-assisted backhaul operation in 5G mmWave cellular networks," *IEEE J. Sel. Areas Commun.*, vol. 36, no. 11, pp. 2486–2496, 2018.

[14] J. Sabzehali, V. K. Shah, H. S. Dhillon, and J. H. Reed, "3D placement and orientation of mmWave-based UAVs for guaranteed LoS coverage," *IEEE Wireless Commun. Lett.*, vol. 10, no. 8, pp. 1662–1666, 2021.

[15] G. Niu, Q. Cao, and M. Pun, "Block diagonal hybrid precoding and power allocation for QoS-aware BDMA downlink transmissions," *Sensors*, vol. 20, no. 16, p. 4497, 2020.

[16] Z. Xiao, H. Dong, L. Bai, D. O. Wu, and X.-G. Xia, "Unmanned aerial vehicle base station (UAV-BS) deployment with millimeter-wave beamforming," *IEEE Internet Things J.*, vol. 7, no. 2, pp. 1336–1349, 2019.

[17] S. Kumar, S. Suman, and S. De, "Dynamic resource allocation in UAV-enabled mmWave communication networks," *IEEE Internet Things J.*, vol. 8, no. 12, pp. 9920–9933, 2020.

[18] Z. Chen, N. Zhao, D. K. C. So, J. Tang, B. Tang, X. Zhang, and K. K. Wong, "Joint altitude and hybrid beamspace precoding optimization for UAV-enabled multiuser mmWave MIMO System," *IEEE Trans. Veh. Technol.*, pp. 1–1, 2021.

[19] D. Hong, S. Lee, Y. H. Cho, D. Baek, J. Kim, and N. Chang, "Least-energy path planning with building accurate power consumption model of rotary unmanned aerial vehicle," *IEEE Trans. Veh. Technol.*, vol. 69, no. 12, pp. 14 803–14 817, 2020.

[20] Y. Zeng, J. Xu, and R. Zhang, "Energy minimization for wireless communication with rotary-wing UAV," *IEEE Trans. Wireless Commun.*, vol. 18, no. 4, pp. 2329–2345, 2019.

[21] Y. Shi, E. Alsusa, and M. W. Baidas, "Energy-efficient decoupled access scheme for cellular-enabled UAV communication systems," *IEEE Systems J.*, pp. 1–12, 2021.

[22] Z. Chen, J. Tian, H. Liu, J. Yu, and X. Chen, "Novel pattern-diverse millimeter-wave antenna with broadband, high-gain, enhanced-coverage for energy-efficient unmanned aerial vehicle," *IEEE Trans. Veh. Technol.*, vol. 70, no. 5, pp. 4081–4087, 2021.

[23] Z. Kang, C. You, and R. Zhang, "3D placement for multi-UAV relaying: An iterative Gibbs-sampling and block coordinate descent optimization approach," *IEEE Trans. Commun.*, vol. 69, no. 3, pp. 2047–2062, 2021.

[24] Y. Sun, D. Xu, D. W. K. Ng, L. Dai, and R. Schober, "Optimal 3D-trajectory design and resource allocation for solar-powered UAV communication systems," *IEEE Trans. Commun.*, vol. 67, no. 6, pp. 4281–4298, 2019.

[25] X. Song, Z. Chang, X. Guo, P. Wu, and T. Hämäläinen, "Energy efficient optimization for solar-powered UAV communications system," in *Proc. IEEE Int. Conf. Commun. Workshops (ICC Workshops)*, 2021, pp. 1–6.

[26] U. Demir, M. Ç. İpek, C. Toker, and Ö. Ekici, "Energy-efficient rotary-wing UAV deployment under flight dynamics and QoS constraints," in *Proc. IEEE Int. Black Sea Conf. Commun. Networking (BlackSeaCom)*, 2019, pp. 1–5.

[27] N. Varshney and S. De, "Multi-RF beamforming-based cellular communication over wideband mmWaves," *IEEE Trans. Commun.*, vol. 70, no. 4, pp. 2772–2787, 2022.

[28] M. Gapeyenko, D. Moltchanov, S. Andreev, and R. W. Heath, "Line-of-sight probability for mmWave-based UAV communications in 3D urban grid deployments," *IEEE Trans. Wireless Commun.*, vol. 20, no. 10, pp. 6566–6579, 2021.

[29] L. N. Ribeiro, S. Schwarz, M. Rupp, and A. L. de Almeida, "Energy efficiency of mmWave massive MIMO precoding with low-resolution DACs," *IEEE J. Sel. Topics Sig. Process.*, vol. 12, no. 2, pp. 298–312, 2018.

[30] A. Basaligheh, P. Saffari, S. Rasti Boroujeni, I. Filanovsky, and K. Moez, "A 28–30 GHz CMOS reflection-type phase shifter with full 360 phase shift range," *IEEE Trans. Circuits and Systems II: Express Briefs*, vol. 67, no. 11, pp. 2452–2456, 2020.

[31] T. Despoisse, "5G 28 GHz high efficiency integrated phased array transceivers," Ph.D. dissertation, Univ. Bordeaux, 2020.

[32] J. Zhang, J. F. Campbell, D. C. Sweeney II, and A. C. Hupman, "Energy consumption models for delivery drones: A comparison and assessment," *Transportation Research Part D: Transport and Environment*, vol. 90, p. 102668, 2021.

[33] C. A. Balanis, *Antenna theory: Analysis and design*. John wiley and sons, 2015.

[34] Y. J. Zhang and K. B. Letaief, "Multiuser adaptive subcarrier-and-bit allocation with adaptive cell selection for OFDM systems," *IEEE Trans. Wireless Commun.*, vol. 3, no. 5, pp. 1566–1575, 2004.

[35] Q. Shi, M. Razaviyayn, Z.-Q. Luo, and C. He, "An iteratively weighted MMSE approach to distributed sum-utility maximization for a MIMO interfering broadcast channel," *IEEE Trans. Sig. Process.*, vol. 59, no. 9, 2011.

[36] A. C. Cirik, O. Taghizadeh, L. Lampe, R. Mathar, and Y. Hua, "Sum-power minimization under rate constraints in full-duplex MIMO systems," in *2016 IEEE 84th Veh. Technol. Conf. (VTC-Fall)*. IEEE, 2016, pp. 1–5.

[37] L. EEMB Co. (2010) Lithium-ion battery data sheet. [Online]. Available: http://eemb.com

[38] Sunpower. (2017) Maxeon solar cells.

[39] A. G. Escobar-Ruiz, O. Lopez-Botello, L. Reyes-Osorio, P. Zambrano-Robledo, L. Amezquita-Brooks, and O. Garcia-Salazar, "Conceptual design of an unmanned fixed-wing aerial vehicle based on alternative energy," *Int. J. Aerospace Eng.*, vol. 2019, 2019.

[40] D. Schnaufer and B. Peterson, "Realizing 5G sub-6-GHzz massive MIMO using GaN," *Microw. RF*, 2018.

[41] H. Shakhatreh, A. Khreishah, and B. Ji, "UAVs to the rescue: Prolonging the lifetime of wireless devices under disaster situations," *IEEE Trans. Green Commun. and Netw.*, vol. 3, no. 4, pp. 942–954, 2019.

[42] Y. Liu and J. Wang, "Low-complexity ofdm-based hybrid precoding for multiuser massive mimo systems," *IEEE Wireless Commun. Lett.*, vol. 9, no. 3, pp. 263–266, 2019.

Nancy Varshney received the B.Tech. degree in Electronics and Communication Engineering from Dr. A.P.J. Abdul Kalam Technical University, Lucknow, India, in 2015, and the M.Tech. degree from Indian Institute of Technology BHU, Varanasi, India, in 2018. She is currently pursuing the Ph.D. degree from Bharti School of Telecommunication, at Indian Institute of Technology Delhi, New Delhi, India. She is a recipient of the Best Paper Awards presented at the National Conference on Communications, 2021. She has been awarded MediaTek-India Research 2022 Fellowship. Her current research interests include beamforming, mmWave communications, UAV communications, and RIS communications.

Swades De [(S'02-M'04-SM'14)] is a Professor in the Department of Electrical Engineering at IIT Delhi. Before moving to IIT Delhi in 2007, he was a Tenure-Track Assistant Professor of Electrical and Computer Engineering at the New Jersey Institute of Technology (2004-2007). He worked as an ERCIM post-doctoral researcher at ISTI-CNR, Pisa, Italy (2004), and has nearly five years of industry experience in India on telecom hardware and software development (1993-1997, 1999). His research interests are broadly in communication networks, with emphasis on performance modeling and analysis. Current directions include energy harvesting sensor networks, broadband wireless access and routing, cognitive/white-space access networks, smart grid networks, and IoT communications. Dr. De currently serves as an Area Editor for the IEEE COMMUNICATIONS LETTERS and Elsevier Computer Communications, and an Associate Editor for the IEEE TRANSACTIONS ON VEHICULAR TECHNOLOGY, the IEEE WIRELESS COMMUNICATIONS LETTERS, and the IEEE NETWORKING LETTERS.